Journal of The Electrochemical Society, **159** (3) F42-F47 (2012)
0013-4651/2012/159(3)/F42/6/$28.00 © The Electrochemical Society

Study of the Catalytic Following Reaction by Scanning Electrochemical Microscopy (SECM)

R. L. Calhoun[a,*,z] **and A. J. Bard**[b,**]

[a] *Chemistry Department, United States Naval Academy, Annapolis, Maryland 21402, USA*
[b] *Department of Chemistry and Biochemistry, The University of Texas at Austin, Austin, Texas 78712, USA*

Scanning electrochemical microscopy (SECM) experiments were undertaken to study the EC′ mechanism, e.g. where a product of the electrode reaction reacts to regenerate the starting material. Digital simulations of the two dimensional SECM were carried out and the results tested with the known EC′ system of $Fe(CN)_6^{4-}$/cysteine for validation. The results were then used in SECM experiments with $Ru(phen)_2dppz^{2+}$, a known DNA intercalator, to study the instability of the oxidized form in the absence and presence of DNA.
 [DOI: 10.1149/2.056203jes]

Manuscript submitted October 24, 2011; revised manuscript received November 21, 2011. Published January 6, 2012. This was Paper 2012 presented at the Montreal, QC, Canada, Meeting of the Society, May 1–6, 2011.

SECM is an electrochemical technique that brings a sharpened ultramicro electrode (UME) within a few tip radii of a substrate to interrogate either solution species or the substrate itself. The basic theory is outlined by Bard et al.[1] One useful aspect of the SECM is that kinetic information of an electrochemical system may be obtained by analyzing the tip and substrate current responses at close distances. Bi et al. showed that a rate constant for a homogenous electron transfer reaction following an electrode reaction may be estimated based on the distance between the tip and the substrate.[2] The collection efficiency (CE), i.e. substrate current/tip current, decreased at larger distances in this situation due to the diffusing species being intercepted by the homogeneous reaction and therefore unable to be converted back at the substrate. Given diffusion time may be estimated by d^2/D where D is the diffusion coefficient of the species in question, finding the nearest distance where CE approached zero gave a time required to consume the diffusing species and, inversely, a rate constant for that reaction.

To aid in discussing various electrochemical reaction schemes, a systematic format for describing heterogeneous electron transfer reactions and homogeneous following chemical reactions has been used for some time.[3] The two that are germane to this work are EC_i and EC′. Here, E refers to the reversible electron transfer reaction that occurs at the electrode and C describes a following chemical reaction in solution. In the former, the subscript denotes this step is irreversible. Thus,

$$R - 1e\text{-} \rightarrow O \text{ (the reversible E step)} \quad [1]$$

followed by

$$O + Y \rightarrow X \text{ (the irreversible C step)} \quad [2]$$

The superscript in the second case (said 'EC prime') denotes this step is catalytic in that the original electroactive species is regenerated. Thus, after 1, the homogeneous reaction 3 follows.

$$O + Y \rightarrow R + X \quad [3]$$

SECM literature is replete with examples of validation of the theoretical model such as the current responses to the experiment above, by using digital simulation. The ECE, and DISP1 reactions are treated in this manner[4] as are the EC_i and EC_{2i} pathways.[5] In this work, the EC′ mechanism is simulated using COMSOL's Multiphysics and validation of the simulation was accomplished by comparison of results to the known EC′ system of ferrocyanide/cysteine.

Using the information obtained, the behavior of $Ru(phen)_2dppz^{3+/2+}$ both free and intercalated into DNA was studied. The rate constant of EC′ following reactions were determined by comparison to digital simulation results. Though theoretical EC′ work for a UME tip has been done,[6] only very recently has the SECM been turned to this reaction scheme in a paper by Unwin accepted after this abstract was submitted to the ECS for presentation at the Spring 2011 meeting.[7] While our approaches are similar, different chemical systems are used.

Experimental

Digital simulation.— COMSOL Multiphysics[8] couples a number of mathematical algorithms for solving differential equations with a multidimensional, user defined, graphical representation of the experimental arrangement. The symmetry of the SECM experiment lends itself well to a two dimensional rendering, which keeps the computational requirements reasonable and is how the data was generated. Simulations were carried out on a Dell Dimension 8400 with 1 GB of RAM and a single 2.8 GHz processor.

Synthesis and materials.— The synthesis of $Ru(phen)_2dppz^{2+}$ began by making $Ru(phen)_2Cl_2 \cdot 2H_2O$ as described by Meyer.[9] The dppz ligand was made separately according to Summers[10] and mated to the parent analogous to Belser's preparation of $Ru(bpy)_2dppz^{2+}$.[11] For the cysteine/ferrocyanide study, cysteine (free base, Sigma-Aldrich), potassium ferrocyanide (Fisher), sodium borate (Baker), and potassium chloride (Baker) were used as received. The buffer of 0.1 M borate was initially ∼ pH 9.5 and was adjusted to pH 11 by adding 2 M NaOH and monitoring with a pH meter.

The 20-mer poly dA-dT was synthesized by Integrated DNA Technologies, Coralville, IA. The solid was dissolved to roughly 3×10^{-4} M in PBS pH 7.5, separated into five 1 mL aliquots and frozen as recommended by the manufacturer until needed. The actual concentration was determined by UV-Vis absorption at 260 nm, using an extinction coefficient of 6300 M^{-1} cm^{-1} for the 20-mer.[12]

The Pt disk ultramicroelectrode (UME) SECM tip (radius, a, nominally 12 μm) in glass was prepared as previously published.[13] The RG was ∼2 and the microscopically measured disk radius and RG were consistent with SECM measurement with ferrocene methanol. The Pt substrate was a locally manufactured disk in glass with an area of 0.013 cm^2. A CH Instruments 900 SECM was used to conduct the approaches and subsequent kinetic experiments.

Results and Discussion

Boundary conditions.— In order to define the boundary conditions of the simulation, relevant equations must first be determined. As an example, the proposed pathway for the $(L)_3Ru^{II}$ complex's reaction would generically be:

$$\text{At tip}: \quad (L)_3Ru^{II} - 1e\text{-} \Leftrightarrow (L)_3Ru^{III} \quad [4]$$

* Electrochemical Society Active Member.
** Electrochemical Society Fellow.
z E-mail: calhoun@usna.edu

$$\text{In solution :} \quad (L)_3Ru^{III} + X \rightarrow (L)_3Ru^{II} + Y \qquad [5]$$

$$\text{At substrate :} \quad (L)_3Ru^{III} + 1e\text{-} \Leftrightarrow (L)_3Ru^{II} \qquad [6]$$

and if X is present in large concentration, a pseudo first order kinetic treatment is possible.[14] Defining the flux equations at the appropriate boundary simulates a diffusion controlled electrode process, and Multiphysics then used a finite element differential equation solver to obtain for the concentration profile at that boundary. For 4, the electrode oxidation reaction, the inward flux of $(L)_3Ru^{II}$ to the tip is defined as:

$$(k_{ft}{}^*[(L)_3Ru^{II}]) - (k_{bt}{}^*[(L)_3Ru^{III}]) \qquad [7]$$

where k_{ft} is the rate constant for the forward reaction at the tip. The flux of Ru^{III} away from the tip is simply the negative of the above expression. The rate constant is further defined as:

$$k_{ft} = k^{o*} \exp(-\alpha f \eta) \qquad [8]$$

where k^o is the heterogeneous electron transfer rate constant, α as the 'transfer coefficient' that arises in the Butler-Volmer treatment of electrode kinetics,[15] f is the inverse of RT/F which is 38.92 V^{-1} at room temperature, and $\eta = E - E^\circ$ for the electrode process in question. Similarly, k_{bt} is the rate constant for the back reaction and is:

$$k_{bt} = k^{o*} \exp[(1 - \alpha f \eta] \qquad [9]$$

Current is derived by integrating the solution of the temporal, two dimensional spatial concentration profiles for the species of interest at the appropriate boundary (either the tip or substrate), i.e.:

$$i = nFA \int [(L)_3Ru^{II} \text{ or } (L)_3Ru^{III}](x, t) \qquad [10]$$

The flux and current at the substrate use the same equation. A voltammogram is generated by using a time dependent solver and making the tip potential a function of time:

$$E_t(t) = E_i + \nu t \qquad [11]$$

where E_i is the initial potential, ν the scan rate in V/s, and t the elapsed time of the sweep.

Simulated voltammetric results.— Initial efforts were made to completely simulate a simple cyclic voltammetry experiment where the voltage is linearly ramped to a maximum value and swept back to the original starting value. However, there were significant difficulties in smoothly solving the temporal concentration profiles when making the sweep reverse so only the sweep out was simulated. Steady state UME current at the end of the sweep out was the correct value but the complete voltammogram still showed slight discontinuities. Efforts to fix this with finer mesh values were unsuccessful due to computer memory limitations. Consequently, a simple chronoamperometric response was simulated with a step to 1.4 V and taking the steady state current after 8s. The agreement in steady state current between the two treatments was within 10 picoamps.

Next, an approach curve was generated by obtaining the simulated tip current at various normalized distance (L = separation distance/tip radius) values and compared with the well-established theory found in Bard and Mirkin (Figure 1). The tip current values are quite close, and the substrate values approach 100% collection efficiency as L drops below 2 as expected.[16] In addition to the unperturbed situation, Multiphysics' predictions for the EC*i* mechanism were compared to published results[17] and performed quite well.

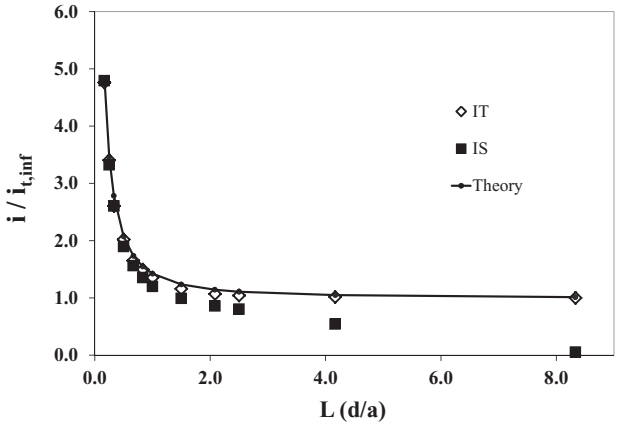

Figure 1. Multiphysics' simulated SECM tip current (IT) and substrate current (IS) compared to established theory for the tip.

EC' modeling.— With confidence the simulation could reproduce the familiar behavior of an SECM experiment in the positive feedback or TGSC mode; results were obtained by adding a following, pseudo first order, catalytic reaction given by 5, generating working curves for various rate constants of that reaction. The rate equations used in the simulation for the homogeneous following reactions in solution are given by:

$$\partial[(L)_3Ru^{III}]/dt = -k_{fol}\,[(L)_3Ru^{III}] \qquad [12]$$

and since it is catalytic,

$$\partial[(L)_3Ru^{II}]/dt = k_{fol}\,[(L)_3Ru^{II}] \qquad [13]$$

The catalytic following reaction was inserted into the simulation and sample substrate current values were obtained for various following reaction rate constants (k_{fol}) as shown in Figure 2. As the following reaction rate constant increased, the amount of $(L)_3Ru^{II}$ regenerated increased and therefore drove the tip current up. This effect is termed catalytic to distinguish it from the term feedback which is used when the returning $(L)_3Ru^{II}$ is generated by the substrate i.e. a homogenous process vs. a heterogeneous process. Note how repeatedly smaller amounts of $(L)_3Ru^{III}$ diffused across the gap for a faster following reaction resulting in smaller substrate currents. Alternately, the distance for the substrate feedback to overcome the following reaction interception of $(L)_3Ru^{III}$ was closer and closer as k_{fol} increased as expected at the outset.

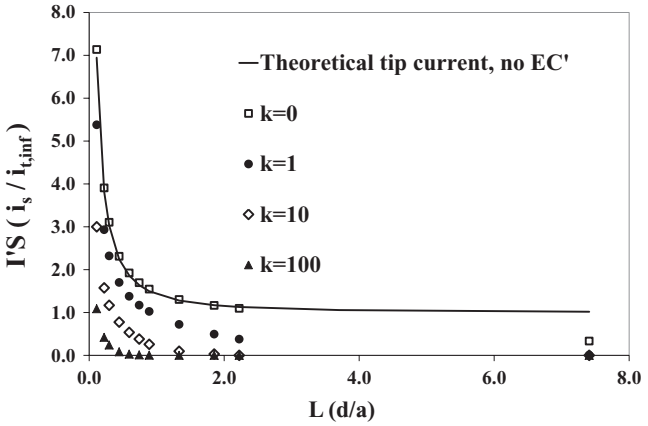

Figure 2. Simulated substrate response as a function of following reaction rate constant as the SECM tip gets closer.

It was less clear how the response would compare to the unperturbed situation once inside this close distance. Comparing Figure 2 to Figure 1 shows that any following reaction decreased the feedback at all distances. This, of course ignores tunneling between the electrodes at very small separations. While this might seem reasonable upon introspection for the substrate, it was surprising for the tip which would be receiving $(L)_3Ru^{III}$ from two sources.

Simulation validation.— With the work done comparing the predictions from Multiphysics to previous, simpler mechanistic systems, a comparison of Multiphysics' predictions to a known EC′ system was the final step required to complete validation of the simulation. Due to its simplicity and aqueous environment, a system of ferrocyanide, $Fe(CN)_6^{4-}$, with the amino acid cysteine was chosen.[18] This system involves the electrochemical oxidation of the cyanide complex of Fe(II) (ferrous) complex to Fe(III) (ferric). Two ferric complexes then oxidize cysteine to cystine which then dimerizes irreversibly and ferrous complexes are regenerated. Additionally, the ferrous/ferric electrode reaction (0.27 V vs. Ag/AgCl) occurs outside the potential window for significant cysteine oxidation (0.8 V vs. SCE)[19] at the electrode, so there should be no significant current from that reaction obscuring the catalytic current of the complex. Also, the reduction of cysteine occurs around 0 V vs. NHE (−0.2 V vs. Ag/AgCl) depending on pH and electrode material,[20] so the substrate may be held at a potential positive enough to avoid significant rates for that reaction as well. This allowed for an SECM scheme as follows:

$$\text{At tip}: \quad Fe(CN)_6^{4-} - 1e\text{-} \rightarrow Fe(CN)_6^{3-} \qquad [14]$$

$$\text{In solution}: \quad 2Fe(CN)_6^{3-} + 2Cys \rightarrow Cys - Cys + 2Fe(CN)_6^{4-} \qquad [15]$$

$$\text{At substrate}: \quad Fe(CN)_6^{3-} + 1e\text{-} \rightarrow Fe(CN)_6^{4-} \qquad [16]$$

It is important to note this system is second order. That is, the rate law for the regeneration of Fe^{2+} is:

$$\text{Rate} = k_{EC'}\,[Fe(CN)_6^{3-}][Cys] \qquad [17]$$

Thus, the rate may be varied by varying the cysteine concentration. For this work, based on data from ref. 18, the rates used ranged from 0.8 to 5.8 mM/s since the reported rate constant at pH 10 is $8 \times 10^3\ M^{-1}s^{-1}$.

Voltammetry.— Initially, cyclic voltammograms were conducted with just the iron complex, and the electroactive radius of the ultramicroelectrode was verified via Eq. 18.

$$I_{ss} = 4nFDCa \qquad [18]$$

where D is the diffusion coefficient, C the concentration, and a the electroactive radius. This radius was modeled into Multiphysics, and predictions of steady state tip currents at large tip/substrate separations (>300 μm) obtained. The simulation was repeated for various solutions of constant Fe(II) concentration and increasing cysteine concentration. Then, solutions of the same composition as those simulated were tested. Steady state currents were obtained by both cyclic voltammogram and chronoamperometry (single potential step). The CVs were conducted from 0.1 to 0.45 V vs. Ag/AgCl at 50 mV/s, and the step experiment was done for 8 s at 0.45 V. Results were reproducible between methods and were in good agreement with the simulations as shown in Figure 3.

Next, approach curves with just ferrocyanide were obtained which fit well to theory for a tip with an RG of 1.5. However, electrode fouling was a problem after spending several minutes producing steady state current once cysteine was added. These approach curves did not agree well with expectations. To solve this problem, an approach was made to substrate contact with just the ferrocyanide to determine how close the tip could be placed. Then the tip was slowly retracted to 30 μm, the cell rinsed, and the solution changed to the equimolar solution. Multiple steps were made back to the substrate, and a CV taken at each distance to obtain the steady state current. Between moves, a cleaning step to −1.3 V was performed, and the data in Figure 4 was obtained. Replicates were completed by backing out and repeating the step-wise approach. Reproducibility and agreement with the simulation was good in the triplicate measurements shown.

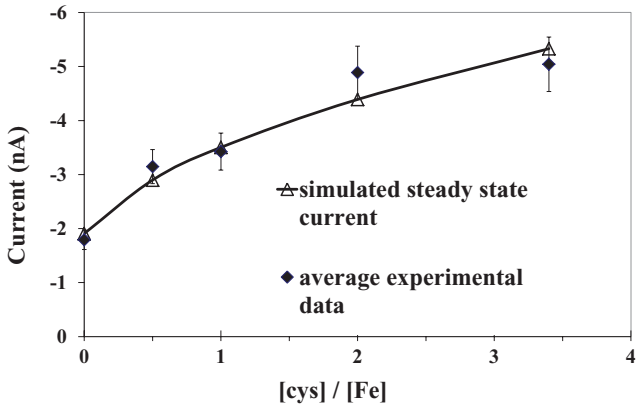

Figure 3. Simulated and experimental tip current for 0.454 mM ferricynide and cysteine system. The experiment was conducted at pH 10.2 which has a published rate constant of $8 \times 10^3\ M^{-1}\ s^{-1}$. That rate constant was subsequently used in the simulation.

$Ru(phen)_2dppz^{2+}$ oxidation in water.— Attempts to study this complex as an electrogenerated chemiluminescent (ECL) agent with DNA were frustrated by below expected stability in aqueous solution. With the work outlined above in hand, elucidation of its behavior both with and without DNA was attempted with the SECM. The experiments shown in Figure 5 showed the $E_{1/2}$ to be 1.23 V vs. Ag/AgCl in the buffered solution; this was a bit of data unattainable via other techniques attempted and was about 100 mV negative of a drybox experiment with very dry acetonitrile.

Current vs. distance data showed significant, negative deviation from the case of no following reaction in both air saturated and

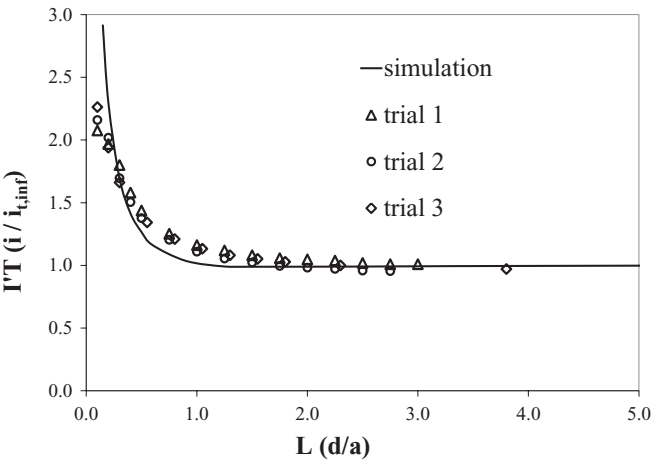

Figure 4. Simulated and actual approach curve data (three trials) for 0.454 mM ferricynide and cysteine.

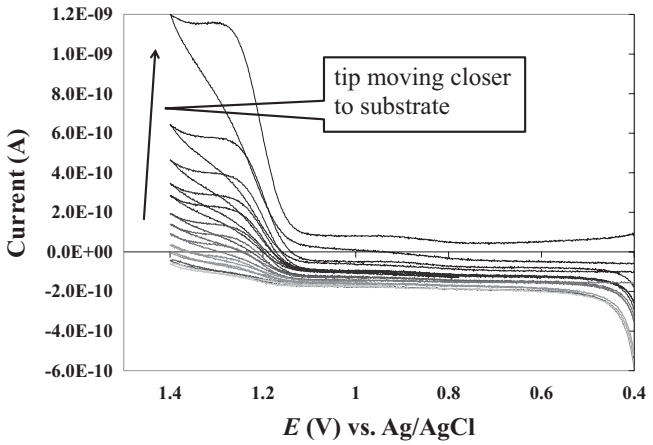

Figure 5. Substrate response of 0.192 mM $Ru(phen)_2dppz^{2+}$ oxidation in 0.1 M PBS, pH 7.5. Responses shown at <1 tip radius for a 25 μm diameter Pt tip.

degassed experiments. Figure 6 shows the poor collection efficiency inside L = 2 indicating the $(L)_3Ru^{III}$ species was undergoing a reaction prior to reaching the substrate even in the absence of DNA. Since the results in degassed solution were very close to those obtained in air saturated solution, the reaction was either with water, water oxidation products or the $(L)_3Ru^{III}$ species is patently unstable. However, the drybox electrochemistry ruled out the latter so a redox reaction is the most probable event.

The case for a direct reaction with water by oxidized ruthenium complexes has some precedent. Most of those studied are oxo-bridged ruthenium dimers,[21,22] but some homonuclear cases have been reported.[23,24] The homonuclear Ru complexes cited are oxidized by Ce(IV) instead of at an electrode, so data from an electrochemical scheme was scarce. Direct evidence for either scheme was not available in the current data. Whatever the event occurring, a following reaction was evident, and one possibility for this was a catalytic reaction where $(L)_3Ru^{II}$ would be regenerated.

Addition of DNA.— The study of electron transfer up and down the helix has demonstrated that intercalated metal complexes may act as oxidizing agents of nucleotide bases (NB), so this was considered a possibility.[25,26] The difference between the 20-mer poly dA-dT data and the calf thymus (not shown) experiments also supports this because CT DNA has GC base pairs as well AT, and guanine has a much lower oxidation potential than A or T.[27] A a stronger driving force for

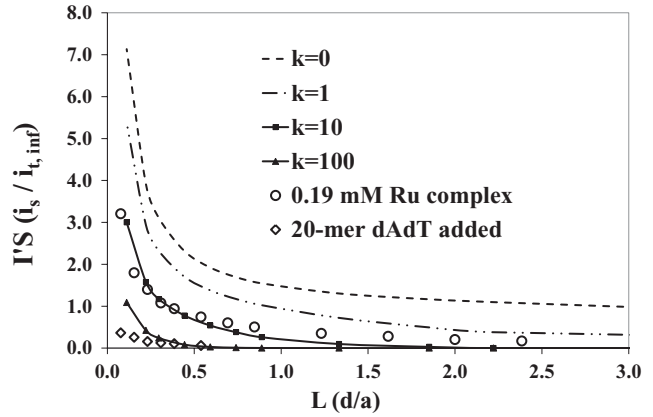

Figure 6. Comparison of $Ru(phen)_2dppz^{2+}$ substrate approach data with (open squares) and without (open circles) DNA added. Working curves for various catalytic rate constants are included for comparison.

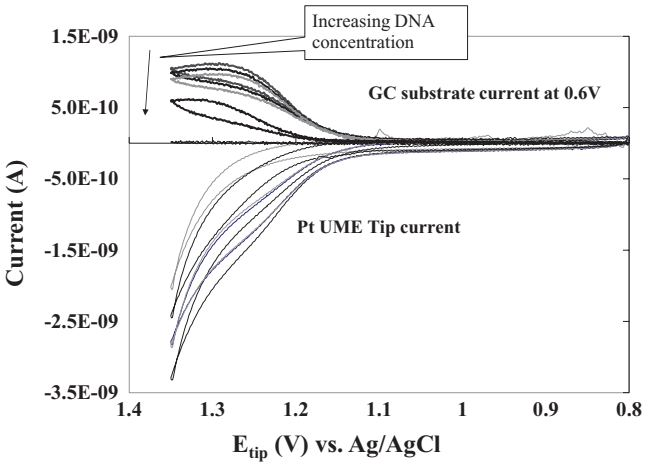

Figure 7. Tip and substrate response of 0.192 mM $Ru(phen)_2dppz^{2+}$ as 20 mer dA-dT is added. The solution was 0.1 M PBS, pH 7.5, R ([base pairs]/[complex]) ranged from 0 to 0.135 and the tip was at 4 μm from the substrate. Note the decreasing tip current corresponds to increased DNA concentration.

the reaction results:

$$(L)_3Ru^{III} + NB \rightarrow (L)_3Ru^{II} + NB_{ox} \quad [19]$$

where NB_{ox} is the oxidized nucleotide base in the helix.

Preliminary work showed $Ru(phen)_2dppz^{2+}$ oxidizes some 230 mV more positive than $Ru(bpy)_3^{2+}$ and is much less soluble in water. Therefore background processes – primarily water oxidation – precluded obtaining meaningful cyclic voltammograms as Thorp showed to verify his argument that guanine is reducing the complex.[28] To overcome this limitation, the SECM was used to determine if adenosine/thymine were reducing $Ru(phen)_2dppz^{3+}$ back to the divalent species.

To probe this possibility, the tip was placed close to the substrate and small volumes of 20-mer poly dA-dT were added to the SECM cell with $Ru(phen)_2dppz^{2+}$ already present. The wait time was 10 minutes after all additions to allow the polynucleotide time to diffuse into the gap and the complex to intercalate. In multiple experiments, at both Pt and GC substrates, the addition of the 20-mer caused significant loss of collected $(L)_3Ru^{III}$. As Figure 7 shows, even at small R values ([base pairs]/[Ru]), the amount of $(L)_3Ru^{III}$ surviving diffusion down to the substrate was significantly lowered by the presence of nucleotides.

While there was a small amount of dilution upon addition of the 20-mer aliquots, the volumes amounted to only 6% over the initial range of R ([base pairs]/[Ru]) values studied. Since the current is directly proportional to the concentration (Eq. 18), that would result in a reduction in current of the same magnitude. The same can be said for the diffusion coefficient. The 20-mer dA-dT has a diffusion coefficient about 60% less than the complex, but at the maximum R value shown, only about 10–15% of the complex was intercalated and therefore exhibited this diffusion coefficient. The rest was free complex. Therefore, the overall current should show very little impact due to intercalated complex if that were the only issue at work. However, the reduction in current is 60% indicating another unidentified process is taking place.

It was considered the electrode surface was being fouled by organic oxidation products. Noting the tip current in Figure 7 was decreasing in concert with the substrate response; this could be an alternate explanation. Additional experiments up to saturating amounts of 20-mer (R = 10.1) were attempted to observe the feedback response with the entire amount of complex intercalated. In these experiments, an electrode cleaning step was added as discussed with cysteine. In this case, a step to −1.3 V vs. Ag/AgCl was done for 20 seconds just prior to performing the cyclic voltammetry but he results were the same. The collection efficiency became negligible at R values >3.

Kinetic estimates.— Using the method for estimating the kinetics of an intervening process in an SECM experiment as outlined in the introduction, the rate constant of the following reaction may be determined by realizing that the time to diffuse across the gap between the tip and substrate (t_{diff}) is given by[29]

$$t_{diff} \sim d^2/D \quad [20]$$

A pseudo first order rate law assuming water is the catalyst and thus present in great excess would be:

$$\text{rate} = k^*_{fol}[(L)_3Ru^{III}] \quad [21]$$

Since the following reaction is in competition with the substrate for $(L)_3Ru^{III}$, the rate constant in Eq. 21 may be estimated by

$$k_{fol} = 1/t_{diff} \quad [22]$$

and the time for $(L)_3Ru^{III}$ to diffuse across the gap represents a time faster than that required to take part in the reaction. So, to enter Eq. 20, a distance where the substrate starts to significantly collect $(L)_3Ru^{III}$ is found. Inspection of Figure 6 shows this occurred for the results without added 20-mer poly dA-dT beginning at L = 0.4. Since this experiment used a 13.8 μm radius tip, that L value corresponds to a tip/substrate separation of 5.5 μm and, via Eq's 20 and 22, k_{fol} may be estimated as 24 s^{-1} which is in good agreement with the working curves generated by the simulation shown in Figure 6.

The process with DNA is more complicated, since the substrate response represents current from both intercalated and free complex and less than saturating amounts of 20-mer were added. However, an estimate of the total effect may be done in the same manner. Given that less than significant collection was occurring even at L = 0.1, a lower estimate of that process was 360 s^{-1}, again reasonable when comparing to Figure 7. Further, if the pseudo first order process is converted to a second order rate equation (since the 20-mer is not present in great excess), then:

$$k_{fol} = k'_{fol}\,[dA - dT] \quad [23]$$

and k'_{fol} is estimated at $\sim 10^6$ $M^{-1}s^{-1}$. This may seem large compared to Thorp's value for $Ru(bpy)_3{}^{2+}$ with the guanine present in calf thymus DNA of 7×10^5 $M^{-1}s^{-1}$.[30] However, there is a distinct difference in that study compared to the current study with $Ru(phen)_2dppz^{2+}$. $Ru(bpy)_3{}^{2+}$ is not an intercalator but rather electrostatically binds to the phosphate backbone. This requires the electron transfer between the base and the complex to occur at greater distances and therefore a slower rate. Since $Ru(phen)_2dppz^{2+}$ literally inserts the dppz ligand in between base pairs, the proximity of reactants should translate into a larger rate constant for the electron transfer.

The significant drop in both tip and substrate current was reasonably due to additional scavenging of the Ru^{III} by the 20-mer. The aqueous redox potentials of adenine and thymine have been interpolated as 1.28 V and 1.26 V vs. NHE at pH 7.5 based on a table published by Faraggi et al.[31] Converting these to potentials vs. Ag/AgCl, values for both bases were around 1 V, well negative of the 1.24 V for $Ru(phen)_2dppz^{3+}$ reported earlier. Thus, the bases were at least thermodynamically amenable to oxidation by the complex.

The additional reduction in collected current could occur due to additional binding of the complex. Electrostatic interactions at low *R* values have also been reported by Hiort et al.[32] Any amount of additional complex binding would subsequently result in slower diffusion and therefore show reduced collected current due to less tip current. The magnitude of this was, however, not defined. In the end, it was not possible to separate these two potential effects that account for the significantly reduced substrate collection current in this experiment.

$(L)_3Ru^{III}$ and $(L)_3Ru^{II}$ binding differences.— Also of note in Figure 7, is the half wave potential was shifted more positive as DNA was added. A blank trial with DNA but no complex was run in both experiments to ensure no electrochemistry of the 20-mer poly dA-dT was occurring and is the zero substrate current trace in Figure 7. Since these blanks confirm no adenosine or thymine electrochemical oxidation, the shift in half-wave potential was due to intercalation of the complex. Bard and Carter have used this information to estimate of the ratio of binding constants for the $(L)_3Ru^{II}$ and $(L)_3Ru^{III}$ species.[33,34] While the complete extent of binding difference was unknown due to no collection seen at saturation levels of the 20-mer, a positive trend in the half wave potential was obvious. A minimum figure was available based on the data taken and the following:

$$E^o_b - E^o_f = 0.059 \log (K_{(L)3RuII}/K_{(L)3RuIII}) \quad [24]$$

which is simply an application of the Nernst equation. Using information from Figure 7, where the average $\Delta E_{1/2}$ is +30 mV from the free complex to the bound complex, the $(L)_3Ru^{II}$ was bound 3× more strongly than $(L)_3Ru^{III}$ at a minimum. These results were not surprising given the similar conclusions of previously studied, analogous complexes. Bard and then Thorp interpreted the results as indicative of a strong interaction between the complex and the hydrophobic core of the DNA helix. The inference was that increasing the charge state of the complex decreases the binding in cases where the complex binds primarily via hydrophobic interactions.

Conclusions

Use of COMSOL's Multiphysics for the simulation of several SECM experiments has been shown to be successful. The data produced for the unperturbed, EC*i*, and EC′ mechanisms have been shown to agree well with experimental data from known systems. A comparison of the simulated EC′ data to the experimental data with $Ru(phen)_2dppz^{2+}$ is shown in Figure 7 which allows an estimate of the rate constants of catalytic following reactions both free and intercalated. This data agrees well with determinations made from tip/substrate separation data (24 s^{-1} and 360 s^{-1}).

Acknowledgment

Financial support was from the National Science Foundation and United States Naval Academy. Special thanks, to Dr. Bill Durham, University of Arkansas, for his advice on ruthenium complex synthesis.

References

1. A. Bard and M. Mirkin, *Scanning Electrochemical Microscopy*, Marcel Dekker, New York (2001).
2. S. Bi, B. Liu, F. Fan, and A. Bard, *J. Am. Chem. Soc.*, **127**, 3690 (2005).
3. A. Testa and W. Reinmuth, *Anal. Chem.*, **33**, 1320 (1961).
4. (a) A. Bard, M. Mirkin, P. Unwin, and D. Wipf, *J. Phys. Chem.*, **96**, 1861 (1992). (b) C. Demaille, P. Unwin, and A. Bard, *J. Phys. Chem.*, **100**, 14137 (1996). (c) R. Martin and P. Unwin, *J. Chem. Soc., Faraday Trans.*, **94**, 753 (1998).
5. (a) P. Unwin and A. Bard, *J. Phys. Chem.*, **95**, 7814 (1991). (b) F. Zhou, P. Unwin, and A. Bard, *J. Phys. Chem.*, **96**, 4917 (1991).
6. L. Rajendran and M. Sanaranarayanan, *J. Phys. Chem. B*, **103**, 1518 (1999).
7. S. Cannan, J. Cervera, R. Steliaros, E. Bitziou, A. Whitworth, and P. Unwin, *Phys. Chem. Chem Phys.*, **13**, 5403 (2011).
8. http://www.comsol.com/products/multiphysics/
9. B. Sullivan, D. Salmon, and T. Meyer, *Inorg Chem.*, **17**, 3334 (1978).
10. J. Dickeson and L. Summers, *Aust J. Chem.*, **23**, 1023 (1970).
11. J. Belser, *Hel. Chem. Acta*, **63**, 1675 (1980).
12. G. Fasman, *CRC Handbook of Biochemistry and Molecular Biology, 3rd Ed. Nucleic Acids Vol 1*, p. 590, CRC Press: Boca Raton, FL, (1975).
13. C. Zoski, *Electroanalysis*, **14**, 1041 (2002).
14. http://www.iupac.org/goldbook/O04322.pdf
15. A. Bard and L. Faulkner, *Electrochemical Methods: Fundamentals and Applications*, 2nd ed., pp. 95–98, John Wiley & Sons, New York, (2001).
16. A. Bard and M. Mirkin, *Scanning Electrochemical Microscopy*, p. 6, Marcel Dekker, New York, (2001).
17. D. Terichel, M. Mirkin, and A. Bard, *J. Phys. Chem.*, **98**, 5751 (1994).
18. O. Nekrassova, G. Allen, N. Lawrence, L. Jiang, G. Jones, and R. Compton, *Electroanalysis*, **14**, 1464 (2002).
19. R. Guo, Z. Li, and T. Liu, *Coll. Poly. Sci.*, **283**, 243 (2004).
20. T. Moehl, A. El Halim, and H. Tributsch, *J. Appl. Electrochem.*, **36**, 1341 (2006).
21. K. Okamoto, J. Miyawaki, K. Nagai, D. Matsumura, A. Nojima, T. Yokoyama, H. Kondoh, and T. Ohta, *Inorg. Chem.*, **42**, 8682 (2003).
22. H. Yamada, T. Koike, and J. Hurst, *J. Am. Chem. Soc.*, **123**, 12775 (2001).

23. M. Yagi, N. Sukegawa, and M. Kaneko, *J. Phys. Chem. B.*, **104**, 4111 (2000).
24. R. Zong and R. Thummel, *J. Am. Chem. Soc.*, **127**, 12802 (2005).
25. J. Yoo, E. Delaney, D. Stemp, and J. Barton, *J. Am. Chem. Soc.*, **125**, 6640 (2003).
26. M. Sistare, R. Holmberg, and H. Thorp, *J. Phys. Chem. B*, **103**, 10718 (1999).
27. M. Faraggi, F. Broitman, J. Trent, and M. Klapper, *J. Phys. Chem.*, **100**, 14751 (1996).
28. M. Sistare, R. Holmberg, and H. Thorp, *J. Phys. Chem. B*, **103**, 10718 (1999).
29. A. Bard and M. Mirkin, *Scanning Electrochemical Microscopy*, p. 10, Marcel Dekker, New York, (2001).
30. D. Johnston and H. Thorp, *J. Phys. Chem.*, **100**, 13837 (1996).
31. M. Faraggi, F. Broitman, J. Trent, and M. Klapper, *J. Phys. Chem.*, **100**, 14751 (1996).
32. C. Hiort, P. Lincoln, and B. Norden, *J. Am. Chem. Soc.*, **115**, 3448 (1993).
33. M. Carter and A. Bard, *J. Am. Chem. Soc.*, **109**, 7528 (1987).
34. M. Carter, M. Rodriguez, and A. Bard, *J. Am. Chem. Soc.*, **111**, 8901 (1989).